INSTITUTE OF PHYSICS PUBLISHING JOURNAL OF PHYSICS B: ATOMIC, MOLECULAR AND OPTICAL PHYSICS

J. Phys. B: At. Mol. Opt. Phys. **34** (2001) 4401–4415 PII: S0953-4075(01)26028-3

Electron-impact excitation of Ne^+

D C Griffin[1], **D M Mitnik**[1] **and N R Badnell**[2]

[1] Department of Physics, Rollins College, Winter Park, FL 32789, USA
[2] Department of Physics and Applied Physics, University of Strathclyde, Glasgow G4 0NG, UK

Received 11 June 2001, in final form 4 October 2001
Published 12 November 2001
Online at stacks.iop.org/JPhysB/34/4401

Abstract

We present the results of a 61-term, 138-level intermediate-coupling frame-transformation R-matrix close-coupling calculation of the electron-impact excitation of fluorine-like Ne^+. All levels of the $2s^22p^5$, $2s2p^6$, $2s^22p^43\ell$ and $2s^22p^44\ell$ configurations that lie below the ionization limit are included in the close-coupling expansion. With the exception of several R-matrix calculations of excitation between the fine structure levels of $2s^22p^5\ ^2P$, this represents the first close-coupling calculation for this ion. Here we describe this calculation and present radiative rates and effective collision strengths for a selected number of the 9453 transitions resulting from this work. The full set of data is available at the Oak Ridge National Laboratory Controlled Fusion Atomic Data Center Web site.

1. Introduction

Data for the electron-impact excitation of the ions of Ne are of significant importance to both laboratory and astrophysical plasmas. For example, Ne is used to cool the impurity plasma in the divertor chamber of magnetic fusion plasmas and reliable collision rates for Ne ions are required for the interpretation of the spectra emitted by a wide variety of gaseous and planetary nebula. In our previous paper, we reported on extensive R-matrix close-coupling calculations for C-like Ne^{4+} [1]. In this paper, we present the results of a large-scale R-matrix calculation for F-like Ne^+.

To date, close-coupling calculations of electron-impact excitation of Ne^+ have been restricted to the fine-structure transition: $2s^22p^5\ ^2P_{3/2} \rightarrow {}^2P_{1/2}$. Johnson and Kingston [2] and later Saraph and Tully [3] employed large configuration-interaction (CI) expansions of the target, but included only the two LS terms $2s^22p^5\ ^2P$ and $2s2p^6\ ^2S$ in their close-coupling expansion; they then employed the program JAJOM [4] to transform the scattering matrices from LS to intermediate coupling and thereby determine the collision strengths for the fine-structure transition.

The present calculations were performed using the intermediate-coupling frame-transformation (ICFT) R-matrix [5] method, for which the close-coupling expansion included the 61 terms and 138 levels of the configurations $2s^22p^5$, $2s2p^6$, $2s^22p^43\ell$, and $2s^22p^44\ell$

that lie below the ionization limit. With the ICFT method, one first employs multi-channel quantum-defect theory (MQDT) to generate 'unphysical' K-matrices in pure LS coupling [6]. These matrices are then transformed to intermediate coupling using term-coupling coefficients, and finally, the physical K-matrices are determined from the unphysical K-matrices and the level energies using MQDT. This has been shown to avoid the problems associated with the term-coupling transformation of physical K-matrices, as is done in the program JAJOM [4] and yields results in excellent agreement with a full Breit–Pauli R-matrix calculation [5, 7]. Here we present our results for effective collision strengths as well as dipole radiative rates for selected transitions in this ion. The effective collision strengths for all 9453 transitions between the 138 levels included in the present calculation, as well as radiative rates for all dipole-allowed transitions are available on the internet at the Oak Ridge National Laboratory (ORNL) Controlled Fusion Atomic Data Center (CFADC)[3].

The remainder of this paper is organized as follows. In the next section, we describe our structure and scattering calculations for this ion. In section 3, we present our results for energies, as well as radiative rates and effective collision strengths for selected transitions. In section 4, we provide a brief summary of our findings.

2. Description of the calculations

2.1. Target-state calculations

The bound-state radial wavefunctions employed in our scattering calculations were generated using Froese Fischer's multi-configuration Hartree–Fock (MCHF) programs [8]. The 1s, 2s, 2p and 3s orbitals were determined from a configuration-average Hartree–Fock (CAHF) calculation on the $2s^22p^43s$ configuration, while the 3p, 3d, 4s, 4p, 4d and 4f orbitals were generated from frozen-core CAHF calculations on the $2s^22p^4n\ell$ configurations. We also included three pseudo-orbitals in order to partially correct the spectroscopic orbitals for variations between configurations. A $\overline{5}$s pseudo-orbital was generated from a MCHF calculation in which the energy of the $2s2p^6\ ^2S$ term was minimized and in which the $2s2p^6\ ^2S$, $2p^63s\ ^2S$, $2p^64s\ ^2S$ and $2p^6\overline{5}s\ ^2S$ terms were included. $\overline{5}$p and $\overline{5}$d pseudo-orbitals were determined from a MCHF calculation in which the energy of the $2s^22p^5\ ^2P$ term was minimized and in which the $2s^22p^5\ ^2P$, $2s^22p^43p\ ^2P$, $2s^22p^44p\ ^2P$, $2s^22p^4\overline{5}p\ ^2P$, $2s2p^53d\ ^2P$, $2s2p^54d\ ^2P$ and $2s2p^5\overline{5}d\ ^2P$ terms were included.

This set of orbitals was then employed in a large Breit–Pauli CI calculation. It included the odd parity levels arising from the $2s^22p^5$, $2s^22p^43p$, $2s^22p^44p$, $2s^22p^44f$, $2s^22p^4\overline{5}p$, $2s2p^53d$, $2s2p^54d$, $2s2p^5\overline{5}d$, $2p^63p$ and $2s^22p^3\overline{5}d^2$ configurations and the even parity levels originating from the configurations $2s2p^6$, $2s^22p^43s$, $2s^22p^43d$, $2s^22p^44s$, $2s^22p^44d$, $2s^22p^4\overline{5}d$, $2s2p^53p$, $2s2p^54p$, $2s2p^5\overline{5}p$, $2p^63s$, $2p^63d$, $2p^64s$, $2p^6\overline{5}s$ and $2s2p^4\overline{5}d^2$.

2.2. Scattering calculations

Here we describe our calculations of ordinary collision strengths and effective collision strengths for the electron-impact excitation of Ne^+ using the ICFT R-matrix method. We first performed an R-matrix calculation with exchange in LS coupling. The close-coupling expansion included all 61 terms of the $2s^22p^5$, $2s2p^6$, $2s^22p^43s$, $2s^22p^43p$, $2s^22p^43d$, $2s^22p^44s$, $2s^22p^44p$, $2s^22p^44d$ and $2s^22p^44f$ configurations that are bound. The size of the R-matrix box was 34.8 au, we used 36 basis orbitals to represent the continuum for each value of the angular momentum and all $LS\Pi$ partial waves from $L = 0$ to 12 were included. We generated

[3] http://www-cfadc.phy.ornl .gov/data_and_codes

unphysical K-matrices in LS coupling using MQDT and then employed the ICFT method to transform the unphysical K-matrices to intermediate coupling; finally, we generated the physical K-matrices in intermediate coupling for all $J\Pi$ partial waves from $J = 0$ to 10. In order to improve on the accuracy of the scattering calculations, the theoretical target energies were adjusted to the experimental values.

In these calculations, we used a number of different energy meshes. In the region between the $2s^2 2p^5\ ^2P_{3/2}$ ground level and the $2s2p^6\ ^2S_{1/2}$ excited level, we employed a mesh spacing that varied between 4.95×10^{-3} Ry and 4.75×10^{-4} Ry, depending on whether or not there were resonance contributions. In the region between the $2s2p^6\ ^2S_{1/2}$ excited level and the highest bound level, we employed a constant energy-mesh spacing of 1.36×10^{-4} Ry. Finally, above all thresholds, we employed an energy-mesh spacing of 3.0×10^{-2} Ry up to a total energy of 6 Ry. This resulted in a total of 8800 energy points. In order to determine whether this mesh resolved the dominant resonance contributions, we performed the following test. We eliminated resonances for which the resonance peak occurred at a single mesh point and was more than a factor of ten greater than the background cross section. We then compared the effective collision strengths calculated with and without this elimination of unresolved resonances and found that they differed by more than 10% in only 26 of the 9453 possible transitions. This indicates that our calculation is converged with respect to the energy mesh.

A $J\Pi$ partial-wave expansion up to $J = 10$ is not sufficiently complete for the determination of collision strengths up to an energy of 6 Ry. Thus we performed an R-matrix calculation without exchange for all $LS\Pi$ partial waves from $L = 9$ to 40 and then used the ICFT method to generate physical K-matrices in intermediate coupling for all $J\Pi$ partial waves from $J = 11$ to 38. These high-J contributions were then topped-up as follows: the dipole-allowed transitions were topped-up using a method originally described by Burgess [9] for LS coupling and implemented here for intermediate coupling; the non-dipole transitions were topped-up assuming a geometric series in J, using energy ratios, and with a special procedure for handling transitions between nearly degenerate levels based on the degenerate limiting case [10]. Finally, it is important to note that in the asymptotic region, we included the long-range multipole potentials perturbatively for all partial waves.

The effective collision strength, Υ, first introduced by Seaton [11], is defined by the equation

$$\Upsilon_{ij} = \int_0^\infty \Omega(i \rightarrow j) \exp\left(\frac{-\epsilon_j}{kT_e}\right) \mathrm{d}\left(\frac{\epsilon_j}{kT_e}\right), \tag{1}$$

where Ω is the collision strength for the transition from level i to level j and ϵ_j is the continuum energy of the final scattered electron. We employed the integration technique of Burgess and Tully [12] to calculate the effective collision strengths. One must use some approximate technique for that part of the integration in equation (1) above the highest energy for which the collision strengths have been calculated. We employ an interpolation method to the infinite energy limit for the collision strengths as discussed in detail in Whiteford *et al* [13]. We have limited our calculations of effective collision strengths to temperatures of up to 4×10^5 K, so that any errors in these interpolations will have a very minor effect on the effective collision strengths.

3. Results

3.1. Bound-state energies and radiative rates

The energies determined from our Breit–Pauli CI calculations of the Ne^+ target are presented in table 1. They are arranged in the order of the theoretical energies; however, the order

Table 1. Energies in Rydbergs for the levels included in the 138-level ICFT *R*-matrix calculation for Ne^+ relative to the $2s^22p^5\ ^2P_{3/2}$ ground level.

Level no	Level	Energy (Th.)	Energy (Exp.[a])	Diff.	Exp. order
1	$2s^22p^5\ ^2P_{3/2}$	0.0000	0.0000	0.0000	1
2	$2s^22p^5\ ^2P_{1/2}$	0.0071	0.0071	0.0000	2
3	$2s^12p^6\ ^2S_{1/2}$	1.9622	1.9779	−0.0157	3
4	$2s^22p^4(^3P)3s\ ^4P_{5/2}$	2.0568	1.9969	0.0599	4
5	$2s^22p^4(^3P)3s\ ^4P_{3/2}$	2.0614	2.0016	0.0598	5
6	$2s^22p^4(^3P)3s\ ^4P_{1/2}$	2.0642	2.0043	0.0599	6
7	$2s^22p^4(^3P)3s\ ^2P_{3/2}$	2.1044	2.0420	0.0624	7
8	$2s^22p^4(^3P)3s\ ^2P_{1/2}$	2.1099	2.0476	0.0623	8
9	$2s^22p^4(^3P)3p\ ^4P_{5/2}$	2.3058	2.2435	0.0623	9
10	$2s^22p^4(^3P)3p\ ^4P_{3/2}$	2.3079	2.2455	0.0624	12
11	$2s^22p^4(^3P)3p\ ^4P_{1/2}$	2.3095	2.2472	0.0623	13
12	$2s^22p^4(^1D)3s\ ^2D_{3/2}$	2.3255	2.2453	0.0802	11
13	$2s^22p^4(^1D)3s\ ^2D_{5/2}$	2.3255	2.2453	0.0802	10
14	$2s^22p^4(^3P)3p\ ^4D_{7/2}$	2.3258	2.2700	0.0558	14
15	$2s^22p^4(^3P)3p\ ^4D_{5/2}$	2.3288	2.2731	0.0557	15
16	$2s^22p^4(^3P)3p\ ^4D_{3/2}$	2.3311	2.2754	0.0557	16
17	$2s^22p^4(^3P)3p\ ^4D_{1/2}$	2.3324	2.2767	0.0557	17
18	$2s^22p^4(^3P)3p\ ^2D_{5/2}$	2.3427	2.2874	0.0553	18
19	$2s^22p^4(^3P)3p\ ^2D_{3/2}$	2.3473	2.2920	0.0553	19
20	$2s^22p^4(^3P)3p\ ^2S_{1/2}$	2.3599	2.3037	0.0562	20
21	$2s^22p^4(^3P)3p\ ^4S_{3/2}$	2.3602	2.3051	0.0551	21
22	$2s^22p^4(^3P)3p\ ^2P_{3/2}$	2.3812	2.3161	0.0651	22
23	$2s^22p^4(^3P)3p\ ^2P_{1/2}$	2.3821	2.3173	0.0648	23
24	$2s^22p^4(^1S)3s\ ^2S_{1/2}$	2.5614	2.5213	0.0401	28
25	$2s^22p^4(^1D)3p\ ^2F_{5/2}$	2.5747	2.5002	0.0745	24
26	$2s^22p^4(^1D)3p\ ^2F_{7/2}$	2.5750	2.5006	0.0744	25
27	$2s^22p^4(^3P)3d\ ^4D_{7/2}$	2.5945	2.5437	0.0508	31
28	$2s^22p^4(^3P)3d\ ^4D_{5/2}$	2.5952	2.5444	0.0508	32
29	$2s^22p^4(^3P)3d\ ^4D_{3/2}$	2.5961	2.5454	0.0507	33
30	$2s^22p^4(^3P)3d\ ^4D_{1/2}$	2.5970	2.5463	0.0507	34
31	$2s^22p^4(^1D)3p\ ^2P_{3/2}$	2.5992	2.5176	0.0804	26
32	$2s^22p^4(^1D)3p\ ^2D_{3/2}$	2.6011	2.5272	0.0739	29
33	$2s^22p^4(^1D)3p\ ^2D_{5/2}$	2.6012	2.5273	0.0739	30
34	$2s^22p^4(^1D)3p\ ^2P_{1/2}$	2.6014	2.5198	0.0816	27
35	$2s^22p^4(^3P)3d\ ^4F_{9/2}$	2.6046	2.5531	0.0515	35
36	$2s^22p^4(^3P)3d\ ^2D_{5/2}$	2.6056	2.5540	0.0516	37
37	$2s^22p^4(^3P)3d\ ^4F_{7/2}$	2.6061	2.5539	0.0522	36
38	$2s^22p^4(^3P)3d\ ^2D_{3/2}$	2.6071	2.5559	0.0512	38
39	$2s^22p^4(^3P)3d\ ^4P_{1/2}$	2.6088	2.5586	0.0502	40
40	$2s^22p^4(^3P)3d\ ^2F_{7/2}$	2.6098	2.5579	0.0519	39
41	$2s^22p^4(^3P)3d\ ^4F_{5/2}$	2.6101	2.5588	0.0513	41
42	$2s^22p^4(^3P)3d\ ^4P_{3/2}$	2.6106	2.5606	0.0500	43
43	$2s^22p^4(^3P)3d\ ^4F_{3/2}$	2.6117	2.5602	0.0515	42
44	$2s^22p^4(^3P)3d\ ^4P_{5/2}$	2.6119	2.5622	0.0497	45
45	$2s^22p^4(^3P)3d\ ^2F_{5/2}$	2.6138	2.5609	0.0529	44
46	$2s^22p^4(^3P)3d\ ^2P_{1/2}$	2.6150	2.5637	0.0513	46
47	$2s^22p^4(^3P)3d\ ^2P_{3/2}$	2.6184	2.5672	0.0512	47
48	$2s^22p^4(^3P)4s\ ^4P_{5/2}$	2.6205	2.5698	0.0507	48
49	$2s^22p^4(^3P)4s\ ^4P_{3/2}$	2.6238	2.5732	0.0506	49
50	$2s^22p^4(^3P)4s\ ^4P_{1/2}$	2.6264	2.5760	0.0504	50

Table 1. (Continued.)

Level no	Level	Energy (Th.)	Energy (Exp.[a])	Diff.	Exp. order
51	$2s^22p^4(^3P)4s\ ^2P_{3/2}$	2.6330	2.5818	0.0512	51
52	$2s^22p^4(^3P)4s\ ^2P_{1/2}$	2.6381	2.5870	0.0511	52
53	$2s^22p^4(^3P)4p\ ^4P_{5/2}$	2.6979	2.6461	0.0518	53
54	$2s^22p^4(^3P)4p\ ^4P_{3/2}$	2.6998	2.6480	0.0518	54
55	$2s^22p^4(^3P)4p\ ^4P_{1/2}$	2.7018	2.6500	0.0518	55
56	$2s^22p^4(^3P)4p\ ^4D_{7/2}$	2.7032	2.6536	0.0496	56
57	$2s^22p^4(^3P)4p\ ^4D_{5/2}$	2.7058	2.6563	0.0495	57
58	$2s^22p^4(^3P)4p\ ^4D_{3/2}$	2.7086	2.6591	0.0495	58
59	$2s^22p^4(^3P)4p\ ^4D_{1/2}$	2.7102	2.6606	0.0496	59
60	$2s^22p^4(^3P)4p\ ^2D_{5/2}$	2.7105	2.6612	0.0492	60
61	$2s^22p^4(^3P)4p\ ^2D_{3/2}$	2.7144	2.6650	0.0494	61
62	$2s^22p^4(^3P)4p\ ^2S_{1/2}$	2.7156	2.6659	0.0497	62
63	$2s^22p^4(^3P)4p\ ^4S_{3/2}$	2.7161	2.6668	0.0493	63
64	$2s^22p^4(^3P)4p\ ^2P_{3/2}$	2.7380	2.6799	0.0581	64
65	$2s^22p^4(^3P)4p\ ^2P_{1/2}$	2.7400	2.6822	0.0578	65
66	$2s^22p^4(^3P)4d\ ^4D_{7/2}$	2.7986	2.7502	0.0484	66
67	$2s^22p^4(^3P)4d\ ^4D_{5/2}$	2.7991	2.7507	0.0484	67
68	$2s^22p^4(^3P)4d\ ^4D_{3/2}$	2.7999	2.7516	0.0483	68
69	$2s^22p^4(^3P)4d\ ^4D_{1/2}$	2.8009	2.7525	0.0484	69
70	$2s^22p^4(^3P)4d\ ^4F_{9/2}$	2.8022	2.7538	0.0484	70
71	$2s^22p^4(^3P)4d\ ^2F_{7/2}$	2.8032	2.7589	0.0443	75
72	$2s^22p^4(^3P)4d\ ^2D_{5/2}$	2.8036	2.7548	0.0488	72
73	$2s^22p^4(^3P)4d\ ^2D_{3/2}$	2.8046	2.7559	0.0487	73
74	$2s^22p^4(^3P)4d\ ^4P_{1/2}$	2.8048	2.7564	0.0484	74
75	$2s^22p^4(^3P)4f\ ^4F_{9/2}$	2.8062	2.7596	0.0466	77
76	$2s^22p^4(^3P)4f\ ^2F_{7/2}$	2.8062	2.7596	0.0466	78
77	$2s^22p^4(^3P)4f\ ^4F_{7/2}$	2.8063	2.7597	0.0466	80
78	$2s^22p^4(^3P)4f\ ^4F_{5/2}$	2.8063	2.7597	0.0466	82
79	$2s^22p^4(^3P)4f\ ^4F_{3/2}$	2.8068	2.7603	0.0465	84
80	$2s^22p^4(^3P)4f\ ^2F_{5/2}$	2.8068	2.7603	0.0465	85
81	$2s^22p^4(^3P)4f\ ^4G_{11/2}$	2.8072	2.7605	0.0467	87
82	$2s^22p^4(^3P)4f\ ^2G_{9/2}$	2.8072	2.7605	0.0467	86
83	$2s^22p^4(^3P)4d\ ^4F_{7/2}$	2.8074	2.7543	0.0531	71
84	$2s^22p^4(^3P)4f\ ^4D_{1/2}$	2.8075	2.7610	0.0465	89
85	$2s^22p^4(^3P)4f\ ^2D_{3/2}$	2.8076	2.7610	0.0466	90
86	$2s^22p^4(^3P)4d\ ^4P_{3/2}$	2.8079	2.7595	0.0484	76
87	$2s^22p^4(^3P)4d\ ^4F_{5/2}$	2.8081	2.7597	0.0484	81
88	$2s^22p^4(^3P)4d\ ^2P_{1/2}$	2.8086	2.7596	0.0490	79
89	$2s^22p^4(^3P)4d\ ^4P_{5/2}$	2.8092	2.7618	0.0474	91
90	$2s^22p^4(^3P)4d\ ^4F_{3/2}$	2.8092	2.7608	0.0484	88
91	$2s^22p^4(^3P)4d\ ^2F_{5/2}$	2.8111	2.7601	0.0510	83
92	$2s^22p^4(^3P)4f\ ^4D_{3/2}$	2.8121	2.7658	0.0463	93
93	$2s^22p^4(^3P)4f\ ^4D_{5/2}$	2.8121	2.7658	0.0463	94
94	$2s^22p^4(^3P)4f\ ^4G_{9/2}$	2.8124	2.7659	0.0465	95
95	$2s^22p^4(^3P)4f\ ^4G_{7/2}$	2.8124	2.7660	0.0464	96
96	$2s^22p^4(^3P)4d\ ^2P_{3/2}$	2.8126	2.7633	0.0493	92
97	$2s^22p^4(^3P)4f\ ^4D_{7/2}$	2.8130	2.7666	0.0464	97
98	$2s^22p^4(^3P)4f\ ^2D_{5/2}$	2.8130	2.7666	0.0464	98
99	$2s^22p^4(^3P)4f\ ^2G_{7/2}$	2.8152	2.7686	0.0466	99
100	$2s^22p^4(^3P)4f\ ^4G_{5/2}$	2.8152	2.7687	0.0465	100
101	$2s^22p^4(^1S)3p\ ^2P_{3/2}$	2.8201	2.7830	0.0371	103

Table 1. (Continued.)

Level no	Level	Energy (Th.)	Energy (Exp.[a])	Diff.	Exp. order
102	$2s^22p^4(^1S)3p\ ^2P_{1/2}$	2.8204	2.7831	0.0373	104
103	$2s^22p^4(^1D)3d\ ^2P_{3/2}$	2.8516	2.7845	0.0671	105
104	$2s^22p^4(^1D)3d\ ^2P_{1/2}$	2.8518	2.7847	0.0671	106
105	$2s^22p^4(^1D)3d\ ^2G_{7/2}$	2.8518	2.7827	0.0691	102
106	$2s^22p^4(^1D)3d\ ^2G_{9/2}$	2.8518	2.7827	0.0691	101
107	$2s^22p^4(^1D)3d\ ^2S_{1/2}$	2.8559	2.7886	0.0673	107
108	$2s^22p^4(^1D)3d\ ^2D_{5/2}$	2.8589	2.7907	0.0682	108
109	$2s^22p^4(^1D)3d\ ^2D_{3/2}$	2.8591	2.7909	0.0682	109
110	$2s^22p^4(^1D)3d\ ^2F_{5/2}$	2.8634	2.7947	0.0687	110
111	$2s^22p^4(^1D)3d\ ^2F_{7/2}$	2.8635	2.7947	0.0688	111
112	$2s^22p^4(^1D)4s\ ^2D_{3/2}$	2.8757	2.8076	0.0681	113
113	$2s^22p^4(^1D)4s\ ^2D_{5/2}$	2.8757	2.8076	0.0681	112
114	$2s^22p^4(^1D)4p\ ^2F_{5/2}$	2.9546	2.8876	0.0670	114
115	$2s^22p^4(^1D)4p\ ^2F_{7/2}$	2.9548	2.8878	0.0670	115
116	$2s^22p^4(^1D)4p\ ^2D_{3/2}$	2.9623	2.8958	0.0665	118
117	$2s^22p^4(^1D)4p\ ^2D_{5/2}$	2.9624	2.8958	0.0666	117
118	$2s^22p^4(^1D)4p\ ^2P_{3/2}$	2.9641	2.8948	0.0693	116
119	$2s^22p^4(^1D)4p\ ^2P_{1/2}$	2.9648	2.8963	0.0685	119
120	$2s^22p^4(^1D)4d\ ^2G_{7/2}$	3.0526	2.9869	0.0657	121
121	$2s^22p^4(^1D)4d\ ^2G_{9/2}$	3.0526	2.9869	0.0657	120
122	$2s^22p^4(^1D)4d\ ^2P_{3/2}$	3.0528	(2.9871)	—	122
123	$2s^22p^4(^1D)4d\ ^2P_{1/2}$	3.0529	(2.9873)	—	123
124	$2s^22p^4(^1D)4d\ ^2S_{1/2}$	3.0532	(2.9876)	—	124
125	$2s^22p^4(^1D)4d\ ^2D_{5/2}$	3.0555	(2.9898)	—	125
126	$2s^22p^4(^1D)4d\ ^2D_{3/2}$	3.0556	(2.9899)	—	126
127	$2s^22p^4(^1D)4f\ ^2P_{1/2}$	3.0574	2.9941	0.0633	130
128	$2s^22p^4(^1D)4f\ ^2P_{3/2}$	3.0574	2.9941	0.0633	129
129	$2s^22p^4(^1D)4d\ ^2F_{5/2}$	3.0574	2.9918	0.0656	127
130	$2s^22p^4(^1D)4d\ ^2F_{7/2}$	3.0575	2.9918	0.0657	128
131	$2s^22p^4(^1D)4f\ ^2H_{9/2}$	3.0585	2.9950	0.0635	131
132	$2s^22p^4(^1D)4f\ ^2H_{11/2}$	3.0585	2.9950	0.0635	132
133	$2s^22p^4(^1D)4f\ ^2D_{3/2}$	3.0586	2.9953	0.0633	134
134	$2s^22p^4(^1D)4f\ ^2D_{5/2}$	3.0586	2.9953	0.0633	133
135	$2s^22p^4(^1D)4f\ ^2F_{5/2}$	3.0598	2.9964	0.0634	136
136	$2s^22p^4(^1D)4f\ ^2F_{7/2}$	3.0598	2.9964	0.0634	135
137	$2s^22p^4(^1D)4f\ ^2G_{7/2}$	3.0601	2.9967	0.0634	137
138	$2s^22p^4(^1D)4f\ ^2G_{9/2}$	3.0601	2.9967	0.0634	138

[a] Kelly [14]. The energies for levels 122–126 are not known experimentally; the numbers in parentheses for these levels were determined from a comparison of the theoretical and experimental energies for the other $2s^22p^4(^1D)4d$ levels.

of the experimental values are listed in the last column. It should be noted that we have used LS notation throughout to label the levels, based on the largest eigenvector component; however, many of the upper levels are strongly mixed and Kelly [14] has used jK notation for many of these higher levels. For the most part, the agreement between the experimental and theoretical energies is quite good; the largest deviation is 3.5% with the deviations for the vast majority of the levels much smaller than that. As mentioned in the last section, we have adjusted the theoretical energies to the experimental ones in our R-matrix close-coupling calculations. There are only five levels for which there are no experimental energies

($2s^22p^4(^1D)4d\ ^2P$, ^2D and ^2S). For those levels, we adjusted the theoretical values to the values given in parentheses; they were determined from the differences between experiment and theory for the other levels arising from $2s^22p^4(^1D)4d$.

In table 2, we present radiative rates for all possible dipole transitions from the levels of the $2s2p^6$, $2s^22p^43s$ and $2s^22p^43d$ configurations to the two levels of the $2s^22p^5$ ground configuration. Our rates are compared to the rates given in the data for the F-like ions generated using the program CIV3 by Blackford and Hibbert [15], and those from the unpublished calculations available in the MCHF/MCDF Collection on the internet[4]. In table 3, we present some radiative rates for transitions for which there are experimental data. They include transitions from levels of the $2s^22p^43p$ configuration to levels of the $2s^22p^43s$ configuration and from levels of the $2s^22p^43d$ configuration to levels of the $2s^22p^43p$ configuration. These rates are compared to the CIV3 values [15], the values from the MCHF/MCDF Collection and the experimental measurements of Griesmann *et al* [16]. In general there is better agreement between our rates and those from the MCHF/MCDF Collection than between our rates and those from the CIV3 calculations; this is especially true for the weaker transitions. There have been new CIV3 calculations [17] for radiative rates in Ne^+ and they are in better agreement with the values from the MCHF/MCDF collection than those shown in tables 2 and 3.

In figure 1, we show a graphical comparison of the present and MCHF/MCDF Collection radiative rates from both tables 2 and 3. The rates for the majority of transitions are in reasonably good agreement; however, there are some exceptions. We see by examining tables 2 and 3 that these larger differences are primarily concentrated in transitions involving levels that arise from the $2s^22p^4(^3P)3d\ ^4P$, $2s^22p^4(^3P)3d\ ^2P$, $2s^22p^4(^3P)3d\ ^4F$ and $2s^22p^4(^3P)3d\ ^2F$ terms. In fact, the average percentage difference between the present and MCHF/MCDF Collection rates for transitions involving these levels is 50%, while for transitions involving the other levels it is 11%. Clearly there are some differences between these two calculations with respect to the spin–orbit mixing of the quartet and doublet levels originating from these terms, and this has significant effects on these particular radiative rates. However, it should be pointed out that electron-impact excitation collision strengths are not as sensitive to variations in such mixing.

In figure 2, we provide a graphical comparison of the present and experimental radiative rates presented in table 3. The majority of our rates are in reasonable agreement with the experimental values, and most of those with larger differences are for weaker transitions. However, we do notice that, with a few exceptions, our rates are larger than the experimental values.

All the radiative rates presented here were calculated in the length gauge. As a final test of our dipole radiative rate calculations, we compared the rates given in tables 2 and 3, with those calculated in the velocity gauge. The average percentage difference between the rates calculated in these two forms was 20% for the 42 transitions in table 2 and 10% for the 34 transitions in table 3.

3.2. Collision strengths and effective collision strengths

In this section, we provide only a small representative sample of our excitation data. In figure 3, we show the collision strengths and effective collision strengths for the $2s^22p^5\ ^2P_{3/2} \rightarrow 2s^22p^5\ ^2P_{1/2}$ excitation. As indicated in the introduction, this is the only transition for which other close-coupling calculations have been performed. In the lower portion of this figure, we compare our results for the effective collision strengths with those of Johnson and Kingston [2] and Saraph and Tully [3]. The results from Johnston and Kingston are about 8.5%

[4] http:/www.vuse.vanderbilt.edu/∼georgio /html_doc/header.html

Table 2. Ne^+ electric-dipole radiative rates for transitions from the levels of the $2s2p^6$, $2s^22p^43s$ and $2s^22p^43d$ configurations to the levels of the $2s^22p^5$ ground configuration.

Transition	Present[a]	CIV3 [b]	MCHF [c]
$2s2p^6\ ^2S_{1/2}$–$2s^22p^5\ ^2P_{3/2}$	5.75×10^9	7.35×10^9	5.54×10^9
$2s^22p^4(^3P)3s\ ^4P_{5/2}$–$2s^22p^5\ ^2P_{3/2}$	3.42×10^5	3.35×10^5	3.25×10^5
$2s^22p^4(^3P)3s\ ^4P_{3/2}$–$2s^22p^5\ ^2P_{3/2}$	9.62×10^6	7.11×10^6	9.57×10^6
$2s^22p^4(^3P)3s\ ^4P_{1/2}$–$2s^22p^5\ ^2P_{3/2}$	1.25×10^6	4.11×10^5	1.24×10^6
$2s^22p^4(^3P)3s\ ^2P_{3/2}$–$2s^22p^5\ ^2P_{3/2}$	3.79×10^9	3.30×10^9	3.28×10^9
$2s^22p^4(^3P)3s\ ^2P_{1/2}$–$2s^22p^5\ ^2P_{3/2}$	1.51×10^9	6.35×10^8	1.27×10^9
$2s^22p^4(^1D)3s\ ^2D_{5/2}$–$2s^22p^5\ ^2P_{3/2}$	1.67×10^9	1.56×10^9	1.58×10^9
$2s^22p^4(^1D)3s\ ^2D_{3/2}$–$2s^22p^5\ ^2P_{3/2}$	2.45×10^8	2.30×10^8	2.33×10^8
$2s^22p^4(^1S)3s\ ^2S_{1/2}$–$2s^22p^5\ ^2P_{3/2}$	7.35×10^8	4.43×10^8	7.86×10^8
$2s^22p^4(^3P)3d\ ^4D_{5/2}$–$2s^22p^5\ ^2P_{3/2}$	4.98×10^6	3.11×10^5	5.68×10^6
$2s^22p^4(^3P)3d\ ^4D_{3/2}$–$2s^22p^5\ ^2P_{3/2}$	1.55×10^7	1.43×10^6	1.56×10^7
$2s^22p^4(^3P)3d\ ^4D_{1/2}$–$2s^22p^5\ ^2P_{3/2}$	6.84×10^6	8.09×10^5	6.33×10^6
$2s^22p^4(^3P)3d\ ^2D_{5/2}$–$2s^22p^5\ ^2P_{3/2}$	2.78×10^9	3.06×10^9	2.68×10^9
$2s^22p^4(^3P)3d\ ^2D_{3/2}$–$2s^22p^5\ ^2P_{3/2}$	1.07×10^9	1.13×10^9	1.04×10^9
$2s^22p^4(^3P)3d\ ^4P_{1/2}$–$2s^22p^5\ ^2P_{3/2}$	1.71×10^7	3.21×10^6	2.70×10^7
$2s^22p^4(^3P)3d\ ^4F_{5/2}$–$2s^22p^5\ ^2P_{3/2}$	5.53×10^8	8.85×10^6	7.29×10^8
$2s^22p^4(^3P)3d\ ^4F_{3/2}$–$2s^22p^5\ ^2P_{3/2}$	2.26×10^8	2.60×10^6	8.35×10^7
$2s^22p^4(^3P)3d\ ^4P_{3/2}$–$2s^22p^5\ ^2P_{3/2}$	2.40×10^7	1.40×10^7	9.28×10^7
$2s^22p^4(^3P)3d\ ^2F_{5/2}$–$2s^22p^5\ ^2P_{3/2}$	4.25×10^8	2.89×10^8	2.28×10^8
$2s^22p^4(^3P)3d\ ^4P_{5/2}$–$2s^22p^5\ ^2P_{3/2}$	8.85×10^7	6.30×10^7	2.70×10^8
$2s^22p^4(^3P)3d\ ^2P_{1/2}$–$2s^22p^5\ ^2P_{3/2}$	7.44×10^8	5.97×10^8	5.58×10^8
$2s^22p^4(^3P)3d\ ^2P_{3/2}$–$2s^22p^5\ ^2P_{3/2}$	1.40×10^9	8.98×10^8	8.82×10^8
$2s^22p^4(^1D)3d\ ^2P_{3/2}$–$2s^22p^5\ ^2P_{3/2}$	2.51×10^9	1.78×10^9	—
$2s^22p^4(^1D)3d\ ^2P_{1/2}$–$2s^22p^5\ ^2P_{3/2}$	1.10×10^9	7.39×10^8	—
$2s^22p^4(^1D)3d\ ^2S_{1/2}$–$2s^22p^5\ ^2P_{3/2}$	2.86×10^9	2.67×10^9	—
$2s^22p^4(^1D)3d\ ^2D_{5/2}$–$2s^22p^5\ ^2P_{3/2}$	1.63×10^9	9.31×10^8	—
$2s^22p^4(^1D)3d\ ^2D_{3/2}$–$2s^22p^5\ ^2P_{3/2}$	2.84×10^8	1.77×10^8	—
$2s^22p^4(^1D)3d\ ^2F_{5/2}$–$2s^22p^5\ ^2P_{3/2}$	1.20×10^6	8.06×10^5	—
$2s2p^6\ ^2S_{1/2}$–$2s^22p^5\ ^2P_{1/2}$	2.81×10^9	2.60×10^9	2.70×10^9
$2s^22p^4(^3P)3s\ ^4P_{3/2}$–$2s^22p^5\ ^2P_{1/2}$	1.19×10^6	8.15×10^5	1.19×10^6
$2s^22p^4(^3P)3s\ ^4P_{1/2}$–$2s^22p^5\ ^2P_{1/2}$	2.17×10^6	5.66×10^6	1.49×10^6
$2s^22p^4(^3P)3s\ ^2P_{3/2}$–$2s^22p^5\ ^2P_{1/2}$	7.19×10^8	6.25×10^8	6.20×10^8
$2s^22p^4(^3P)3s\ ^2P_{1/2}$–$2s^22p^5\ ^2P_{1/2}$	3.02×10^9	3.40×10^9	2.64×10^9
$2s^22p^4(^1D)3s\ ^2D_{3/2}$–$2s^22p^5\ ^2P_{1/2}$	1.42×10^9	1.33×10^9	1.35×10^9
$2s^22p^4(^1S)3s\ ^2S_{1/2}$–$2s^22p^5\ ^2P_{1/2}$	3.92×10^8	2.21×10^8	4.20×10^8
$2s^22p^4(^3P)3d\ ^4D_{3/2}$–$2s^22p^5\ ^2P_{1/2}$	4.30×10^6	1.16×10^5	7.04×10^6
$2s^22p^4(^3P)3d\ ^4D_{1/2}$–$2s^22p^5\ ^2P_{1/2}$	1.40×10^7	1.75×10^6	1.30×10^7
$2s^22p^4(^3P)3d\ ^2D_{3/2}$–$2s^22p^5\ ^2P_{1/2}$	1.90×10^9	2.05×10^9	2.05×10^9
$2s^22p^4(^3P)3d\ ^4P_{1/2}$–$2s^22p^5\ ^2P_{1/2}$	1.92×10^7	7.62×10^5	2.86×10^7
$2s^22p^4(^3P)3d\ ^4F_{3/2}$–$2s^22p^5\ ^2P_{1/2}$	2.48×10^8	1.04×10^7	1.21×10^7
$2s^22p^4(^3P)3d\ ^4P_{3/2}$–$2s^22p^5\ ^2P_{1/2}$	2.23×10^8	2.45×10^6	4.45×10^8
$2s^22p^4(^3P)3d\ ^2P_{1/2}$–$2s^22p^5\ ^2P_{1/2}$	1.43×10^9	1.10×10^9	1.05×10^9
$2s^22p^4(^3P)3d\ ^2P_{3/2}$–$2s^22p^5\ ^2P_{1/2}$	1.21×10^9	1.00×10^9	9.64×10^8
$2s^22p^4(^1D)3d\ ^2P_{3/2}$–$2s^22p^5\ ^2P_{1/2}$	5.29×10^8	3.73×10^8	—
$2s^22p^4(^1D)3d\ ^2P_{1/2}$–$2s^22p^5\ ^2P_{1/2}$	2.00×10^9	1.49×10^9	—
$2s^22p^4(^1D)3d\ ^2S_{1/2}$–$2s^22p^5\ ^2P_{1/2}$	1.56×10^9	1.37×10^9	—
$2s^22p^4(^1D)3d\ ^2D_{3/2}$–$2s^22p^5\ ^2P_{1/2}$	1.42×10^9	8.11×10^8	—

[a] Calculated using the same CI basis states that were employed to determine the energies in table 1.
[b] Blackford and Hibbert [15].
[c] MCHF/MCDF Collection: www.vuse.vanderbilt.edu/∼georgio/html_doc/header.html

Table 3. Ne^+ electric-dipole radiative rates for transitions from levels of the $2s^22p^43p$ configuration to levels of the $2s^22p^43s$ configuration and from levels of the $2s^22p^43d$ configuration to levels of the $2s^22p^43p$ configuration.

Transition	Present[a]	CIV3 [b]	MCHF [c]	Experiment [d]
$2s^22p^4(^3P)3p\ ^4P_{5/2}$–$2s^22p^4(^3P)3s\ ^4P_{5/2}$	1.15×10^8	1.11×10^8	1.03×10^8	9.47×10^7
$2s^22p^4(^3P)3p\ ^4P_{5/2}$–$2s^22p^4(^3P)3s\ ^4P_{3/2}$	3.04×10^7	3.12×10^7	2.95×10^7	2.70×10^7
$2s^22p^4(^3P)3p\ ^4P_{3/2}$–$2s^22p^4(^3P)3s\ ^4P_{5/2}$	7.95×10^7	8.04×10^7	7.09×10^7	5.53×10^7
$2s^22p^4(^3P)3p\ ^4P_{3/2}$–$2s^22p^4(^3P)3s\ ^4P_{3/2}$	2.19×10^7	1.88×10^7	1.89×10^7	1.47×10^7
$2s^22p^4(^3P)3p\ ^4P_{3/2}$–$2s^22p^4(^3P)3s\ ^4P_{1/2}$	4.44×10^7	4.29×10^7	4.23×10^7	3.16×10^7
$2s^22p^4(^3P)3p\ ^4P_{1/2}$–$2s^22p^4(^3P)3s\ ^4P_{3/2}$	1.26×10^8	1.23×10^8	1.14×10^8	1.02×10^8
$2s^22p^4(^3P)3p\ ^4P_{1/2}$–$2s^22p^4(^3P)3s\ ^4P_{1/2}$	1.88×10^7	1.90×10^7	1.80×10^7	1.57×10^7
$2s^22p^4(^3P)3p\ ^2D_{5/2}$–$2s^22p^4(^3P)3s\ ^4P_{5/2}$	4.70×10^5	1.78×10^5	5.74×10^5	3.88×10^6
$2s^22p^4(^3P)3p\ ^2D_{5/2}$–$2s^22p^4(^3P)3s\ ^4P_{3/2}$	1.80×10^6	4.33×10^5	1.45×10^6	9.25×10^6
$2s^22p^4(^3P)3p\ ^2D_{5/2}$–$2s^22p^4(^3P)3s\ ^2P_{3/2}$	1.46×10^8	1.41×10^8	1.37×10^8	1.12×10^8
$2s^22p^4(^3P)3p\ ^2D_{3/2}$–$2s^22p^4(^3P)3s\ ^4P_{3/2}$	3.78×10^5	1.37×10^5	2.65×10^5	1.23×10^6
$2s^22p^4(^3P)3p\ ^2D_{3/2}$–$2s^22p^4(^3P)3s\ ^4P_{1/2}$	4.57×10^5	1.17×10^5	3.99×10^5	1.98×10^6
$2s^22p^4(^3P)3p\ ^2D_{3/2}$–$2s^22p^4(^3P)3s\ ^2P_{3/2}$	3.30×10^7	1.86×10^7	3.34×10^7	2.89×10^7
$2s^22p^4(^3P)3p\ ^2D_{3/2}$–$2s^22p^4(^3P)3s\ ^2P_{1/2}$	1.15×10^8	1.10×10^8	1.05×10^8	8.70×10^7
$2s^22p^4(^3P)3p\ ^2S_{1/2}$–$2s^22p^4(^3P)3s\ ^2P_{3/2}$	1.36×10^8	1.19×10^8	1.40×10^8	1.58×10^8
$2s^22p^4(^3P)3p\ ^2S_{1/2}$–$2s^22p^4(^3P)3s\ ^2P_{1/2}$	3.43×10^7	4.39×10^7	2.24×10^7	2.52×10^7
$2s^22p^4(^3P)3p\ ^4S_{3/2}$–$2s^22p^4(^3P)3s\ ^4P_{5/2}$	1.16×10^8	1.13×10^8	1.12×10^8	9.67×10^7
$2s^22p^4(^3P)3p\ ^4S_{3/2}$–$2s^22p^4(^3P)3s\ ^4P_{3/2}$	8.90×10^7	9.04×10^7	8.42×10^7	7.63×10^7
$2s^22p^4(^3P)3p\ ^4S_{3/2}$–$2s^22p^4(^3P)3s\ ^4P_{1/2}$	4.92×10^7	5.49×10^7	4.54×10^7	4.20×10^7
$2s^22p^4(^3P)3p\ ^2P_{3/2}$–$2s^22p^4(^3P)3s\ ^2P_{3/2}$	1.55×10^8	1.42×10^8	1.38×10^8	1.35×10^8
$2s^22p^4(^3P)3p\ ^2P_{3/2}$–$2s^22p^4(^3P)3s\ ^2P_{1/2}$	3.95×10^7	3.23×10^7	3.93×10^7	3.96×10^7
$2s^22p^4(^3P)3p\ ^2P_{1/2}$–$2s^22p^4(^3P)3s\ ^2P_{3/2}$	4.24×10^7	5.06×10^7	2.56×10^7	2.36×10^7
$2s^22p^4(^3P)3p\ ^2P_{1/2}$–$2s^22p^4(^3P)3s\ ^2P_{1/2}$	1.48×10^8	1.19×10^8	1.48×10^8	1.62×10^8
$2s^22p^4(^1D)3p\ ^2F_{5/2}$–$2s^22p^4(^1D)3s\ ^2D_{5/2}$	1.14×10^7	1.14×10^7	1.08×10^7	9.89×10^6
$2s^22p^4(^1D)3p\ ^2F_{5/2}$–$2s^22p^4(^1D)3s\ ^2D_{3/2}$	1.49×10^8	1.51×10^7	1.39×10^8	1.22×10^7
$2s^22p^4(^3P)3d\ ^4D_{7/2}$–$2s^22p^4(^3P)3p\ ^4P_{5/2}$	3.03×10^8	3.53×10^8	2.95×10^8	2.70×10^8
$2s^22p^4(^3P)3d\ ^4D_{7/2}$–$2s^22p^4(^3P)3p\ ^4D_{7/2}$	9.00×10^7	1.07×10^8	8.89×10^7	8.58×10^7
$2s^22p^4(^3P)3d\ ^4D_{7/2}$–$2s^22p^4(^3P)3p\ ^4D_{5/2}$	4.53×10^6	1.58×10^6	2.90×10^6	1.08×10^6
$2s^22p^4(^3P)3d\ ^4F_{7/2}$–$2s^22p^4(^3P)3p\ ^4D_{7/2}$	2.24×10^7	3.35×10^7	1.61×10^7	7.64×10^6
$2s^22p^4(^3P)3d\ ^4F_{7/2}$–$2s^22p^4(^3P)3p\ ^4D_{5/2}$	2.26×10^8	3.86×10^8	1.69×10^8	8.56×10^7
$2s^22p^4(^3P)3d\ ^4F_{7/2}$–$2s^22p^4(^3P)3p\ ^2D_{5/2}$	1.07×10^8	2.46×10^5	1.60×10^8	1.20×10^8
$2s^22p^4(^3P)3d\ ^2F_{7/2}$–$2s^22p^4(^3P)3p\ ^4P_{5/2}$	1.97×10^6	2.17×10^6	2.05×10^3	1.33×10^6
$2s^22p^4(^3P)3d\ ^2F_{7/2}$–$2s^22p^4(^3P)3p\ ^4D_{7/2}$	1.16×10^7	6.79×10^4	1.64×10^7	8.46×10^6
$2s^22p^4(^3P)3d\ ^2F_{7/2}$–$2s^22p^4(^3P)3p\ ^4D_{5/2}$	1.11×10^8	1.45×10^5	1.61×10^8	1.11×10^8
$2s^22p^4(^3P)3d\ ^2F_{7/2}$–$2s^22p^4(^3P)3p\ ^2D_{5/2}$	2.29×10^8	3.61×10^8	1.59×10^8	1.12×10^8

[a] Calculated using the same CI basis states that were employed to determine the energies in table 1.
[b] Blackford and Hibbert [15].
[c] MCHF/MCDF Collection: www.vuse.vanderbilt.edu/∼georgio/html_doc/header.html
[d] Griesmann *et al* [16].

higher than our values at the lowest temperatures of 10^3 K, but are in much closer agreement for temperatures above 2.5×10^3 K. On the other hand, the results from Saraph and Tully are in excellent agreement with our values at 10^3 K, but are below our results for the higher temperatures, with a maximum difference of 9.8% at 10^4 K. However, Tully [18] has recently carried-out a three-level Breit–Pauli calculation and obtained results that are about 10% larger than those of Saraph and Tully.

The collision strengths and effective collision strengths for the transitions from both the $2s^22p^5\ ^2P_{3/2}$ ground level and the $2s^22p^5\ ^2P_{1/2}$ excited level to the $2s2p^6\ ^2S_{1/2}$ level are shown

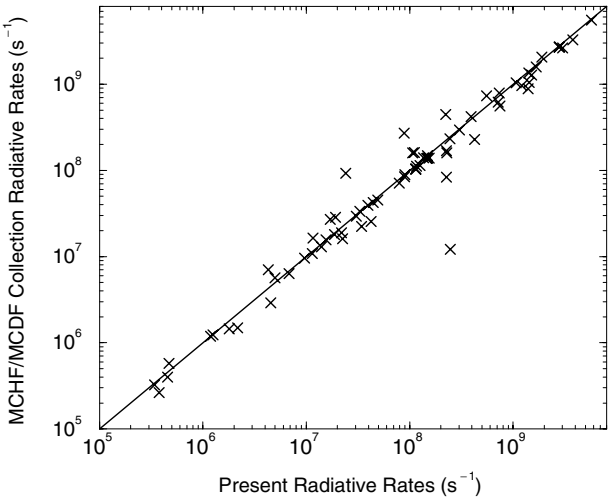

Figure 1. Graphical comparison of the present and MCHF/MCDF Collection electric-dipole radiative rates given in tables 2 and 3.

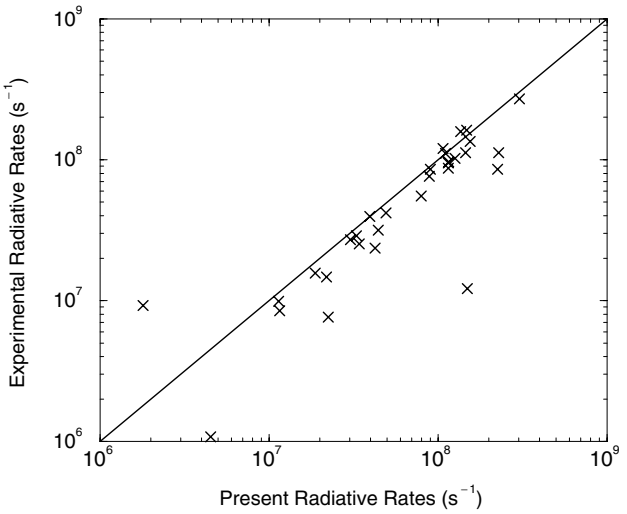

Figure 2. Graphical comparison of the present and experimental electric-dipole radiative rates given in table 3.

in figure 4. Although there are noticeable resonance contributions to the collision strengths for these dipole-allowed transitions, they have a rather small effect on the effective collision strength. This is in contrast to the corresponding curves shown in figure 5 for the transitions from $2s^22p^5\ ^2P_{3/2}$ and $2s^22p^5\ ^2P_{1/2}$ to the $2s^22p^43s\ ^4P_{5/2}$ level. The transition from $2s^22p^5\ ^2P_{1/2}$ is dipole forbidden, while the excitation from $2s^22p^5\ ^2P_{3/2}$ is only weakly dipole allowed. Thus at the lower temperatures, the effective collision strengths for these two transitions are completely dominated by the strong resonance contributions.

In table 4, we present the effective collision strengths for excitation from the $2s^22p^5\ ^2P_{3/2}$ ground level to all 46 levels from $2s^22p^5\ ^2P_{1/2}$ through the highest $2s^22p^4(^3P)3d$ level. In

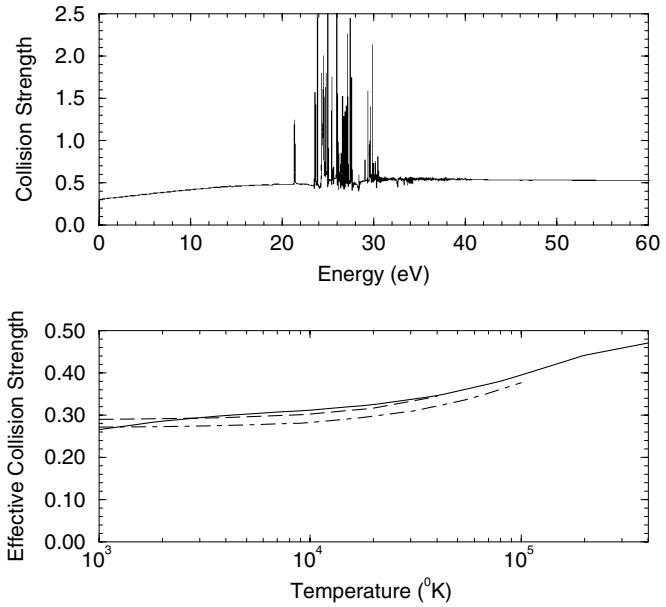

Figure 3. Collision strengths (top) and effective collision strengths (bottom) for excitation from the $2s^22p^5\ ^2P_{3/2}$ ground level to the $2s^22p^5\ ^2P_{1/2}$ excited level. The solid curves are from the present calculation, the dashed curve in the bottom graph is from the fit to the effective collision strength for this transition from the calculation of Johnson and Kingston [2] and the dot-dash curve in that graph is from Saraph and Tully [3].

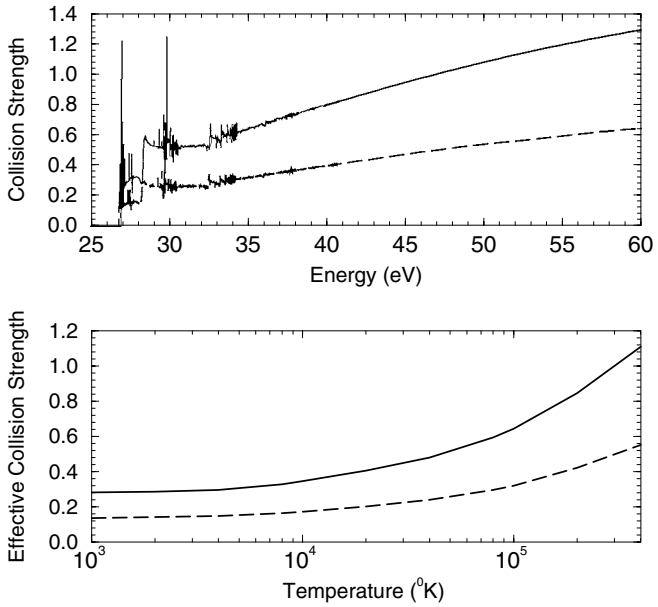

Figure 4. Collision strengths (top) and effective collision strengths (bottom) for excitation from the $2s^22p^5\ ^2P_{3/2}$ ground level (solid curves) and from the $2s^22p^5\ ^2P_{1/2}$ excited level (dashed curves) to the $2s2p^6\ ^2S_{1/2}$ level.

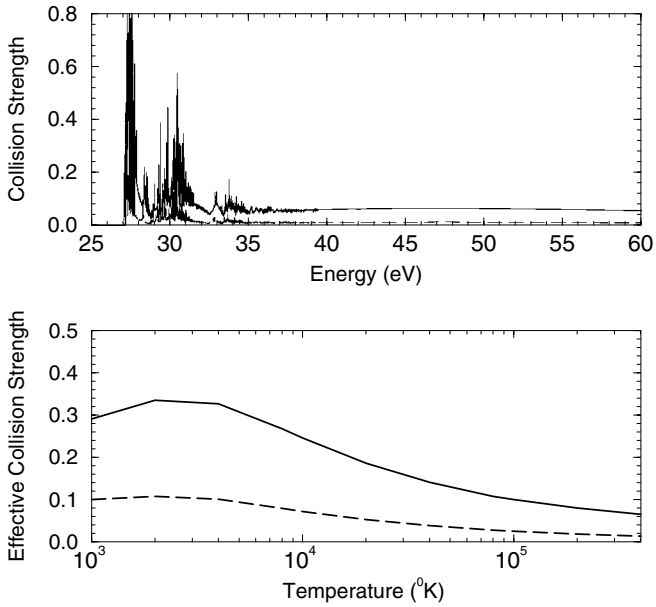

Figure 5. Collision strengths (top) and effective collision strengths (bottom) for excitation from the $2s^22p^5\ ^2P_{3/2}$ ground level (solid curves) and from the $2s^22p^5\ ^2P_{1/2}$ excited level (dashed curves) to the $2s^22p^43s\ ^4P_{5/2}$ level.

table 5, we show the effective collision strengths for excitation from the $2s^22p^5\ ^2P_{1/2}$ excited level to all 45 levels from $2s2p^6\ ^2S_{1/2}$ through the highest $2s^22p^4(^3P)3d$ level. The complete set of effective collision strengths for the 9453 transitions between the 138 levels included in the present study, along with the electric dipole radiative rates tabulated in the ADAS *adf04* format [19], are available via the WWW under http://www-cfadc.phy.ornl.gov/data_and_codes.

It is difficult to estimate the accuracy of large scale effective collision strength calculations; this is especially true in this case where there are no other calculations with which we may make comparisons, beyond those for excitation between the ground-state levels. In general, based on comparisons in other ions, we would expect the collision strengths for the strong dipole-allowed transitions to be accurate to about 20%. However, the effective collision strengths for dipole-forbidden or weakly allowed dipole transitions are normally less accurate. Such transitions are often dominated by resonance contributions, the magnitude of which is more difficult to determine accurately. However, in Ne^+, our energy mesh is sufficiently fine to resolve the dominant resonances, and this reduces the uncertainty in the resonance contributions to the effective collision strengths. In more highly ionized species, resolving these resonances is much more difficult. There is also some uncertainty associated with the dipole top-up for weakly allowed dipole transitions. Of the 9453 transitions included in this study, 778 had top-up contributions of 30% or more of the total and all of these were for weakly allowed dipole transitions.

Even for the stronger dipole transitions, the effective collision strengths to and between the $2s^22p^4(^1S)3p$, $2s^22p^4(^1D)3d$ and $2s^22p^44\ell$ levels should be considered somewhat less accurate than those between the lower levels. This is due to the fact that above level 90 (in experimental order) in table 1, the $2s^22p^4n\ell$ levels with $n > 4$, that are not included in our close-coupling expansion, begin to appear. Thus coupling to the $2s^22p^4n\ell$ levels with $n > 4$, as well as resonance contributions originating from them, will become more important for excitation to

Table 4. Ne^+ effective collision strengths for excitation from the $2s^22p^5\ ^2P_{3/2}$ ground level to all levels up through the highest $2s^22p^4(^3P)3d$ level.

	Electron temperature (K)					
Upper level	1.00×10^3	4.00×10^3	1.00×10^4	4.00×10^4	1.00×10^5	4.00×10^5
$2s^22p^5\ ^2P_{1/2}$	2.66×10^{-1}	2.99×10^{-1}	3.14×10^{-1}	3.50×10^{-1}	4.00×10^{-1}	4.73×10^{-1}
$2s2p^6\ ^2S_{1/2}$	2.83×10^{-1}	2.97×10^{-1}	3.46×10^{-1}	4.81×10^{-1}	6.44×10^{-1}	1.11×10^{0}
$2s^22p^4(^3P)3s\ ^4P_{5/2}$	2.91×10^{-1}	3.27×10^{-1}	2.46×10^{-1}	1.41×10^{-1}	9.99×10^{-2}	6.49×10^{-2}
$2s^22p^4(^3P)3s\ ^4P_{3/2}$	2.22×10^{-1}	1.99×10^{-1}	1.37×10^{-1}	7.49×10^{-2}	5.13×10^{-2}	3.22×10^{-2}
$2s^22p^4(^3P)3s\ ^4P_{1/2}$	1.02×10^{-1}	8.11×10^{-2}	5.41×10^{-2}	2.92×10^{-2}	1.96×10^{-2}	1.16×10^{-2}
$2s^22p^4(^3P)3s\ ^2P_{3/2}$	1.27×10^{-1}	1.37×10^{-1}	1.65×10^{-1}	1.95×10^{-1}	2.38×10^{-1}	4.88×10^{-1}
$2s^22p^4(^3P)3s\ ^2P_{1/2}$	2.95×10^{-2}	3.75×10^{-2}	4.81×10^{-2}	5.37×10^{-2}	5.71×10^{-2}	1.01×10^{-1}
$2s^22p^4(^3P)3p\ ^4P_{5/2}$	1.03×10^{-1}	8.89×10^{-2}	6.87×10^{-2}	4.86×10^{-2}	4.61×10^{-2}	4.38×10^{-2}
$2s^22p^4(^1D)3s\ ^2D_{5/2}$	9.53×10^{-2}	1.08×10^{-1}	1.07×10^{-1}	1.11×10^{-1}	1.29×10^{-1}	2.38×10^{-1}
$2s^22p^4(^1D)3s\ ^2D_{3/2}$	5.68×10^{-2}	6.25×10^{-2}	5.61×10^{-2}	4.87×10^{-2}	4.47×10^{-2}	4.80×10^{-2}
$2s^22p^4(^3P)3p\ ^4P_{3/2}$	5.02×10^{-2}	4.89×10^{-2}	3.79×10^{-2}	2.63×10^{-2}	2.40×10^{-2}	2.17×10^{-2}
$2s^22p^4(^3P)3p\ ^4P_{1/2}$	2.33×10^{-2}	2.22×10^{-2}	1.65×10^{-2}	1.09×10^{-2}	9.47×10^{-3}	8.02×10^{-3}
$2s^22p^4(^3P)3p\ ^4D_{7/2}$	9.34×10^{-2}	7.77×10^{-2}	6.64×10^{-2}	5.26×10^{-2}	4.87×10^{-2}	4.25×10^{-2}
$2s^22p^4(^3P)3p\ ^4D_{5/2}$	5.12×10^{-2}	4.51×10^{-2}	3.91×10^{-2}	3.20×10^{-2}	2.97×10^{-2}	2.63×10^{-2}
$2s^22p^4(^3P)3p\ ^4D_{3/2}$	3.05×10^{-2}	2.47×10^{-2}	2.07×10^{-2}	1.72×10^{-2}	1.60×10^{-2}	1.40×10^{-2}
$2s^22p^4(^3P)3p\ ^4D_{1/2}$	1.39×10^{-2}	1.07×10^{-2}	8.74×10^{-3}	7.31×10^{-3}	6.89×10^{-3}	6.03×10^{-3}
$2s^22p^4(^3P)3p\ ^2D_{5/2}$	8.03×10^{-2}	6.92×10^{-2}	6.39×10^{-2}	5.44×10^{-2}	5.24×10^{-2}	6.61×10^{-2}
$2s^22p^4(^3P)3p\ ^2D_{3/2}$	3.56×10^{-2}	3.14×10^{-2}	2.99×10^{-2}	2.60×10^{-2}	2.46×10^{-2}	3.08×10^{-2}
$2s^22p^4(^3P)3p\ ^2S_{1/2}$	2.06×10^{-2}	1.61×10^{-2}	1.48×10^{-2}	1.32×10^{-2}	1.20×10^{-2}	1.00×10^{-2}
$2s^22p^4(^3P)3p\ ^4S_{3/2}$	2.12×10^{-2}	2.03×10^{-2}	1.98×10^{-2}	1.69×10^{-2}	1.35×10^{-2}	9.78×10^{-3}
$2s^22p^4(^3P)3p\ ^2P_{3/2}$	1.58×10^{-1}	1.75×10^{-1}	1.90×10^{-1}	1.99×10^{-1}	2.29×10^{-1}	3.15×10^{-1}
$2s^22p^4(^3P)3p\ ^2P_{1/2}$	1.31×10^{-2}	1.57×10^{-2}	1.81×10^{-2}	1.70×10^{-2}	1.64×10^{-2}	1.99×10^{-2}
$2s^22p^4(^1D)3p\ ^2F_{5/2}$	3.08×10^{-2}	2.89×10^{-2}	2.80×10^{-2}	2.72×10^{-2}	2.93×10^{-2}	3.14×10^{-2}
$2s^22p^4(^1D)3p\ ^2F_{7/2}$	5.25×10^{-2}	5.15×10^{-2}	4.99×10^{-2}	4.56×10^{-2}	4.70×10^{-2}	5.74×10^{-2}
$2s^22p^4(^1D)3p\ ^2P_{3/2}$	6.41×10^{-2}	6.86×10^{-2}	7.40×10^{-2}	9.07×10^{-2}	1.30×10^{-1}	2.25×10^{-1}
$2s^22p^4(^1D)3p\ ^2P_{1/2}$	1.38×10^{-2}	1.36×10^{-2}	1.25×10^{-2}	1.06×10^{-2}	1.07×10^{-2}	1.13×10^{-2}
$2s^22p^4(^1S)3s\ ^2S_{1/2}$	4.19×10^{-2}	3.72×10^{-2}	3.40×10^{-2}	3.11×10^{-2}	3.08×10^{-2}	3.55×10^{-2}
$2s^22p^4(^1D)3p\ ^2D_{3/2}$	1.94×10^{-2}	2.24×10^{-2}	2.40×10^{-2}	2.38×10^{-2}	2.63×10^{-2}	3.40×10^{-2}
$2s^22p^4(^1D)3p\ ^2D_{5/2}$	2.34×10^{-2}	2.56×10^{-2}	2.68×10^{-2}	2.54×10^{-2}	2.45×10^{-2}	2.36×10^{-2}
$2s^22p^4(^3P)3d\ ^4D_{7/2}$	2.69×10^{-2}	1.89×10^{-2}	1.61×10^{-2}	1.57×10^{-2}	1.99×10^{-2}	2.13×10^{-2}
$2s^22p^4(^3P)3d\ ^4D_{5/2}$	2.20×10^{-2}	1.49×10^{-2}	1.24×10^{-2}	1.15×10^{-2}	1.39×10^{-2}	1.50×10^{-2}
$2s^22p^4(^3P)3d\ ^4D_{3/2}$	1.33×10^{-2}	9.55×10^{-3}	8.06×10^{-3}	7.33×10^{-3}	8.53×10^{-3}	9.18×10^{-3}
$2s^22p^4(^3P)3d\ ^4D_{1/2}$	7.42×10^{-3}	4.97×10^{-3}	4.04×10^{-3}	3.45×10^{-3}	3.78×10^{-3}	3.76×10^{-3}
$2s^22p^4(^3P)3d\ ^4F_{9/2}$	1.38×10^{-2}	1.33×10^{-2}	1.36×10^{-2}	1.41×10^{-2}	1.62×10^{-2}	1.49×10^{-2}
$2s^22p^4(^3P)3d\ ^4F_{7/2}$	1.47×10^{-2}	1.37×10^{-2}	1.37×10^{-2}	1.31×10^{-2}	1.41×10^{-2}	1.40×10^{-2}
$2s^22p^4(^3P)3d\ ^2D_{5/2}$	3.61×10^{-2}	3.69×10^{-2}	3.85×10^{-2}	5.08×10^{-2}	8.77×10^{-2}	2.20×10^{-1}
$2s^22p^4(^3P)3d\ ^2D_{3/2}$	1.58×10^{-2}	1.50×10^{-2}	1.49×10^{-2}	1.76×10^{-2}	2.78×10^{-2}	6.27×10^{-2}
$2s^22p^4(^3P)3d\ ^2F_{7/2}$	1.33×10^{-2}	1.22×10^{-2}	1.20×10^{-2}	1.09×10^{-2}	1.14×10^{-2}	1.16×10^{-2}
$2s^22p^4(^3P)3d\ ^4P_{1/2}$	2.85×10^{-3}	2.38×10^{-3}	2.28×10^{-3}	2.07×10^{-3}	2.29×10^{-3}	2.53×10^{-3}
$2s^22p^4(^3P)3d\ ^4F_{5/2}$	1.28×10^{-2}	1.25×10^{-2}	1.25×10^{-2}	1.43×10^{-2}	2.17×10^{-2}	4.71×10^{-2}
$2s^22p^4(^3P)3d\ ^4F_{3/2}$	6.26×10^{-3}	6.11×10^{-3}	6.10×10^{-3}	6.31×10^{-3}	8.48×10^{-3}	1.55×10^{-2}
$2s^22p^4(^3P)3d\ ^4P_{3/2}$	6.69×10^{-3}	5.72×10^{-3}	5.42×10^{-3}	4.85×10^{-3}	5.28×10^{-3}	5.87×10^{-3}
$2s^22p^4(^3P)3d\ ^2F_{5/2}$	1.34×10^{-2}	1.32×10^{-2}	1.32×10^{-2}	1.34×10^{-2}	1.82×10^{-2}	3.71×10^{-2}
$2s^22p^4(^3P)3d\ ^4P_{5/2}$	1.42×10^{-2}	1.44×10^{-2}	1.41×10^{-2}	1.34×10^{-2}	1.49×10^{-2}	1.80×10^{-2}
$2s^22p^4(^3P)3d\ ^2P_{1/2}$	6.86×10^{-3}	6.72×10^{-3}	6.71×10^{-3}	7.58×10^{-3}	1.11×10^{-2}	2.29×10^{-2}
$2s^22p^4(^3P)3d\ ^2P_{3/2}$	1.65×10^{-2}	1.72×10^{-2}	1.73×10^{-2}	2.19×10^{-2}	3.56×10^{-2}	8.15×10^{-2}

Table 5. Ne^+ effective collision strengths for excitation from the $2s^22p^5\ ^2P_{1/2}$ excited level to all levels up through the highest $2s^22p^4(^3P)3d$ level.

	Electron temperature (K)					
Upper level	1.00×10^3	4.00×10^3	1.00×10^4	4.00×10^4	1.00×10^5	4.00×10^5
$2s2p^6\ ^2S_{1/2}$	1.37×10^{-1}	1.48×10^{-1}	1.73×10^{-1}	2.40×10^{-1}	3.21×10^{-1}	5.52×10^{-1}
$2s^22p^4(^3P)3s\ ^4P_{5/2}$	1.00×10^{-1}	1.01×10^{-1}	7.20×10^{-2}	3.84×10^{-2}	2.50×10^{-2}	1.39×10^{-2}
$2s^22p^4(^3P)3s\ ^4P_{3/2}$	1.31×10^{-1}	1.26×10^{-1}	8.96×10^{-2}	5.01×10^{-2}	3.52×10^{-2}	2.26×10^{-2}
$2s^22p^4(^3P)3s\ ^4P_{1/2}$	8.82×10^{-2}	8.06×10^{-2}	5.67×10^{-2}	3.23×10^{-2}	2.32×10^{-2}	1.53×10^{-2}
$2s^22p^4(^3P)3s\ ^2P_{3/2}$	3.96×10^{-2}	4.01×10^{-2}	4.82×10^{-2}	5.27×10^{-2}	5.63×10^{-2}	9.97×10^{-2}
$2s^22p^4(^3P)3s\ ^2P_{1/2}$	4.42×10^{-2}	5.01×10^{-2}	6.06×10^{-2}	7.30×10^{-2}	9.22×10^{-2}	1.94×10^{-1}
$2s^22p^4(^3P)3p\ ^4P_{5/2}$	2.80×10^{-2}	2.56×10^{-2}	1.92×10^{-2}	1.27×10^{-2}	1.07×10^{-2}	8.70×10^{-3}
$2s^22p^4(^1D)3s\ ^2D_{5/2}$	4.55×10^{-2}	4.91×10^{-2}	4.24×10^{-2}	3.43×10^{-2}	2.92×10^{-2}	2.20×10^{-2}
$2s^22p^4(^1D)3s\ ^2D_{3/2}$	3.83×10^{-2}	4.26×10^{-2}	4.41×10^{-2}	4.93×10^{-2}	6.11×10^{-2}	1.27×10^{-1}
$2s^22p^4(^3P)3p\ ^4P_{3/2}$	3.34×10^{-2}	3.02×10^{-2}	2.31×10^{-2}	1.57×10^{-2}	1.45×10^{-2}	1.35×10^{-2}
$2s^22p^4(^3P)3p\ ^4P_{1/2}$	2.25×10^{-2}	2.13×10^{-2}	1.61×10^{-2}	1.08×10^{-2}	1.02×10^{-2}	9.70×10^{-3}
$2s^22p^4(^3P)3p\ ^4D_{7/2}$	1.99×10^{-2}	1.58×10^{-2}	1.30×10^{-2}	1.08×10^{-2}	1.05×10^{-2}	9.32×10^{-3}
$2s^22p^4(^3P)3p\ ^4D_{5/2}$	2.87×10^{-2}	2.47×10^{-2}	2.11×10^{-2}	1.69×10^{-2}	1.59×10^{-2}	1.41×10^{-2}
$2s^22p^4(^3P)3p\ ^4D_{3/2}$	2.61×10^{-2}	2.30×10^{-2}	1.98×10^{-2}	1.59×10^{-2}	1.46×10^{-2}	1.27×10^{-2}
$2s^22p^4(^3P)3p\ ^4D_{1/2}$	1.64×10^{-2}	1.37×10^{-2}	1.17×10^{-2}	9.28×10^{-3}	8.45×10^{-3}	7.23×10^{-3}
$2s^22p^4(^3P)3p\ ^2D_{5/2}$	2.79×10^{-2}	2.35×10^{-2}	2.18×10^{-2}	1.81×10^{-2}	1.68×10^{-2}	1.99×10^{-2}
$2s^22p^4(^3P)3p\ ^2D_{3/2}$	3.27×10^{-2}	2.94×10^{-2}	2.77×10^{-2}	2.40×10^{-2}	2.31×10^{-2}	2.81×10^{-2}
$2s^22p^4(^3P)3p\ ^2S_{1/2}$	1.00×10^{-2}	8.55×10^{-3}	8.09×10^{-3}	7.46×10^{-3}	6.87×10^{-3}	6.41×10^{-3}
$2s^22p^4(^3P)3p\ ^4S_{3/2}$	1.25×10^{-2}	1.15×10^{-2}	1.09×10^{-2}	9.00×10^{-3}	7.08×10^{-3}	4.97×10^{-3}
$2s^22p^4(^3P)3p\ ^2P_{3/2}$	1.40×10^{-2}	1.69×10^{-2}	1.94×10^{-2}	1.84×10^{-2}	1.80×10^{-2}	2.22×10^{-2}
$2s^22p^4(^3P)3p\ ^2P_{1/2}$	7.44×10^{-2}	8.03×10^{-2}	8.60×10^{-2}	9.00×10^{-2}	1.04×10^{-1}	1.42×10^{-1}
$2s^22p^4(^1D)3p\ ^2F_{5/2}$	2.68×10^{-2}	2.48×10^{-2}	2.33×10^{-2}	2.03×10^{-2}	2.04×10^{-2}	2.65×10^{-2}
$2s^22p^4(^1D)3p\ ^2F_{7/2}$	1.90×10^{-2}	1.78×10^{-2}	1.73×10^{-2}	1.74×10^{-2}	1.91×10^{-2}	1.95×10^{-2}
$2s^22p^4(^1D)3p\ ^2P_{3/2}$	1.71×10^{-2}	1.49×10^{-2}	1.35×10^{-2}	1.17×10^{-2}	1.19×10^{-2}	1.26×10^{-2}
$2s^22p^4(^1D)3p\ ^2P_{1/2}$	2.69×10^{-2}	3.20×10^{-2}	3.60×10^{-2}	4.65×10^{-2}	6.88×10^{-2}	1.22×10^{-1}
$2s^22p^4(^1S)3s\ ^2S_{1/2}$	2.17×10^{-2}	1.92×10^{-2}	1.76×10^{-2}	1.63×10^{-2}	1.63×10^{-2}	1.90×10^{-2}
$2s^22p^4(^1D)3p\ ^2D_{3/2}$	8.43×10^{-3}	8.79×10^{-3}	8.76×10^{-3}	8.33×10^{-3}	8.23×10^{-3}	8.17×10^{-3}
$2s^22p^4(^1D)3p\ ^2D_{5/2}$	1.09×10^{-2}	1.23×10^{-2}	1.31×10^{-2}	1.18×10^{-2}	1.07×10^{-2}	9.67×10^{-3}
$2s^22p^4(^3P)3d\ ^4D_{7/2}$	9.28×10^{-3}	6.32×10^{-3}	5.34×10^{-3}	4.61×10^{-3}	4.85×10^{-3}	4.24×10^{-3}
$2s^22p^4(^3P)3d\ ^4D_{5/2}$	9.52×10^{-3}	6.17×10^{-3}	4.82×10^{-3}	4.14×10^{-3}	4.86×10^{-3}	5.00×10^{-3}
$2s^22p^4(^3P)3d\ ^4D_{3/2}$	8.26×10^{-3}	5.44×10^{-3}	4.19×10^{-3}	3.60×10^{-3}	4.43×10^{-3}	5.15×10^{-3}
$2s^22p^4(^3P)3d\ ^4D_{1/2}$	5.05×10^{-3}	3.30×10^{-3}	2.58×10^{-3}	2.26×10^{-3}	2.87×10^{-3}	3.54×10^{-3}
$2s^22p^4(^3P)3d\ ^4F_{9/2}$	4.04×10^{-3}	3.79×10^{-3}	3.94×10^{-3}	3.82×10^{-3}	4.27×10^{-3}	3.76×10^{-3}
$2s^22p^4(^3P)3d\ ^4F_{7/2}$	5.76×10^{-3}	4.62×10^{-3}	4.47×10^{-3}	3.92×10^{-3}	4.01×10^{-3}	3.93×10^{-3}
$2s^22p^4(^3P)3d\ ^2D_{5/2}$	6.73×10^{-3}	5.07×10^{-3}	4.46×10^{-3}	3.51×10^{-3}	3.44×10^{-3}	3.37×10^{-3}
$2s^22p^4(^3P)3d\ ^2D_{3/2}$	1.45×10^{-2}	1.52×10^{-2}	1.59×10^{-2}	2.11×10^{-2}	3.73×10^{-2}	9.72×10^{-2}
$2s^22p^4(^3P)3d\ ^2F_{7/2}$	7.35×10^{-3}	6.86×10^{-3}	6.79×10^{-3}	6.47×10^{-3}	7.12×10^{-3}	6.97×10^{-3}
$2s^22p^4(^3P)3d\ ^4P_{1/2}$	1.91×10^{-3}	1.72×10^{-3}	1.66×10^{-3}	1.60×10^{-3}	1.94×10^{-3}	2.37×10^{-3}
$2s^22p^4(^3P)3d\ ^4F_{5/2}$	6.31×10^{-3}	6.14×10^{-3}	6.02×10^{-3}	5.89×10^{-3}	6.65×10^{-3}	6.62×10^{-3}
$2s^22p^4(^3P)3d\ ^4F_{3/2}$	5.86×10^{-3}	5.95×10^{-3}	5.95×10^{-3}	6.55×10^{-3}	9.13×10^{-3}	1.67×10^{-2}
$2s^22p^4(^3P)3d\ ^4P_{3/2}$	5.84×10^{-3}	5.45×10^{-3}	5.32×10^{-3}	5.78×10^{-3}	8.22×10^{-3}	1.54×10^{-2}
$2s^22p^4(^3P)3d\ ^2F_{5/2}$	8.91×10^{-3}	8.73×10^{-3}	8.63×10^{-3}	8.09×10^{-3}	8.68×10^{-3}	9.75×10^{-3}
$2s^22p^4(^3P)3d\ ^4P_{5/2}$	5.84×10^{-3}	5.48×10^{-3}	5.25×10^{-3}	4.78×10^{-3}	5.13×10^{-3}	4.77×10^{-3}
$2s^22p^4(^3P)3d\ ^2P_{1/2}$	6.76×10^{-3}	6.88×10^{-3}	6.94×10^{-3}	8.98×10^{-3}	1.56×10^{-2}	3.88×10^{-2}
$2s^22p^4(^3P)3d\ ^2P_{3/2}$	1.34×10^{-2}	1.39×10^{-2}	1.40×10^{-2}	1.74×10^{-2}	2.84×10^{-2}	6.69×10^{-2}

and between these upper levels. Finally, coupling to the target continuum has been shown to have relatively large effects on excitation to the upper levels in much simpler species [20–22]; this is especially true for lower stages of ionization and such continuum coupling effects are not included here.

4. Conclusions

We have performed a 138-level ICFT R-matrix coupling calculation for Ne^+. This represents the first close-coupling calculation for this ion beyond several calculations of the $2s^22p^5\ ^2P_{3/2} \rightarrow 2s^22p^5\ ^2P_{1/2}$ fine-structure transition. The electric-dipole radiative rates determined from our large CI Breit–Pauli calculation are in reasonable agreement with unpublished MCHF calculations available on the WWW as well as the experimental dipole radiative rates determined by Griesmann *et al* [16]. Our effective collision strengths for the $2s^22p^5\ ^2P_{3/2} \rightarrow 2s^22p^5\ ^2P_{1/2}$ fine-structure transition are consistent with the earlier calculations of Johnson and Kingston [2] and Saraph and Tully [3]. The complete set of data necessary for collisional radiative modelling for this ion is available on the WWW at the CFADC site at ORNL.

Acknowledgments

In this work, DCG was supported by a US DoE grant (DE-FG02-96-ER54367) with Rollins College, DMM was supported by a subcontract with Los Alamos National Laboratory and NRB was supported by a UK PPARC grant (PPA/G/S/1997/00783) with the University of Strathclyde. DCG wishes to acknowledge support for his stay as a short-term visitor at the Institute for Theoretical Atomic and Molecular Physics at the Harvard–Smithsonian Center for Astrophysics, where a portion of this work was performed.

References

[1] Griffin D C and Badnell N R 2000 *J. Phys. B: At. Mol. Opt. Phys.* **33** 4389
[2] Johnson C T and Kingston A E 1987 *J. Phys. B: At. Mol. Phys.* **20** 5757
[3] Saraph H E and Tully J A 1994 *Astron. Astrophys. Suppl.* **107** 29
[4] Saraph H E 1978 *Comput. Phys. Commun.* **15** 247
[5] Griffin D C, Badnell N R and Pindzola M S 1998 *J. Phys. B: At. Mol. Opt. Phys.* **31** 3713
[6] Gorczyca T W and Badnell N R 2000 *J. Phys. B: At. Mol. Opt. Phys.* **33** 2511
[7] Griffin D C, Badnell N R, Pindzola M S and Shaw J A 1999 *J. Phys. B: At. Mol. Opt. Phys.* **32** 2139
[8] Froese Fischer C 1991 *Comput. Phys. Commun.* **64** 369
[9] Burgess A 1974 *J. Phys. B: At. Mol. Phys.* **7** L364
[10] Burgess A, Hummer D G and Tully J A 1970 *Phil. Trans. R. Soc.* A **266** 225
[11] Seaton M J 1953 *Proc. R. Soc.* A **218** 400
[12] Burgess A and Tully J A 1992 *Astron. Astrophys.* **254** 436
[13] Whiteford A D, Badnell N R, Ballance C P, O'Mullane M G, Summers H P and Thomas A L 2001 *J. Phys. B: At. Mol. Opt. Phys.* **34** 3179
[14] Kelly R L 1987 *J. Phys. Chem. Ref. Data* (Suppl) **16** 1
[15] Blackford H M S and Hibbert A 1994 *At. Data Nucl. Data Tables* **58** 101
[16] Griesmann U, Musielok J and Wiese W 1997 *J. Opt. Soc. Am.* B **14** 2204
[17] Hibbert A 2001 Private communication
[18] Tully J A 2001 Private communication
[19] Summers H P 1999 *ADAS User Manual Version 2.1* webpage http://adas.phys.strath.ac.uk/
[20] Bartschat K, Hudson E T, Scott M P, Burke P G and Burke V M 1996 *J. Phys. B: At. Mol. Opt. Phys.* **29** 115
[21] Bartschat K and Bray I 1997 *J. Phys. B: At. Mol. Opt. Phys.* **30** L109
[22] Griffin D C, Badnell N R and Pindzola M S 2000 *J. Phys. B: At. Mol. Opt. Phys.* **33** 1013